Journal of Materials Chemistry A

ROYAL SOCIETY OF CHEMISTRY

PAPER

View Article Online
View Journal | View Issue



Cite this: J. Mater. Chem. A, 2024, 12, 4077

# A nonfullerene acceptor as a solid additive realizing a record efficiency of 17.74% in quasi-layered all-polymer solar cells†

Wenjing Xu,‡[a] Miao Zhang, ‡[b] Zhongyuan Liu,[a] Hongyue Tian,[a] Wenqing Zhang,[c] Shixiu Sun,[d] Sang Young Jeong,[e] Fenghua Zhang,[f] Xiong Li,[f] Qianqian Sun, [d] Xiaotao Hao, [c] Han Young Woo, *[e] Xiaoling Ma *[ag] and Fujun Zhang *[a]

Quasi-layered all-polymer solar cells (QLA-PSCs) were fabricated based on wide bandgap polymer PM6 as a donor and narrow bandgap polymer PY-IT as an acceptor. A nonfullerene acceptor, L8-BO, is deliberately selected as a solid additive due to its similar chemical structure to the segment of polymer acceptor PY-IT. The power conversion efficiency (PCE) of the QLA-PSCs is increased from 16.14% to 17.74% by incorporating 2 wt% L8-BO into the PY-IT layer, benefiting from the synergistically increased short circuit current density (24.45 mA $cm^{-2}$ *vs.* 23.41 mA $cm^{-2}$) and fill factor (76.38% *vs.* 72.60%). The contribution of L8-BO as a solid additive on the performance improvement of the QLA-PSCs can be summarized as follows: (i) it induces more ordered molecular orientation of PY-IT confirmed from GIWAXS; (ii) it enlarges the exciton diffusion length in the PY-IT layer and facilitates efficient hole transfer from PY-IT to PM6 as demonstrated by transient absorption; (iii) it increases the exciton dissociation interface as evidenced by the contact angle and photoluminescence of PM6/PY-IT without or with L8-BO. It should be highlighted that the 2000 h storage stability of the QLA-PSCs can be significantly improved, with PCE retention increasing from 85.1% to 90.2% of the initial value upon incorporating L8-BO as a solid additive. The effect of the universality of the nonfullerene acceptor as a solid additive on the performance improvement of QLA-PSCs can also be confirmed by the boosted PCE to 16.71% or 16.79% with Y6 or BO-4F as a solid additive. This work shows that a small molecular nonfullerene acceptor may induce a polymer acceptor molecular arrangement to further improve the performance of QLA-PSCs.

Received 23rd November 2023
Accepted 9th January 2024

DOI: 10.1039/d3ta07228b

rsc.li/materials-a



## Introduction

All-polymer solar cells (all-PSCs) composed of a polymer donor and polymer acceptor have been recognized as one of the most promising photovoltaic technologies due to their exceptional mechanical flexibility and superior film forming features for large-scale production.[1–4] The recent flourishing development of polymer materials, especially for polymerized small molecular acceptors, has driven the power conversion efficiency (PCE) to exceed 18% for bulk-heterojunction (BHJ) configuration all-PSCs, which lags behind that of polymer solar cells made from small molecular nonfullerene acceptors.[5–8] Phase separation and molecular packing regulation are still highly challenging for BHJ configuration all-PSCs due to the strongly tangled polymer chains in mixed donor : acceptor solution.[9,10] Quasi-layered all-polymer solar cells (QLA-PSCs) have aroused attention by employing the sequential spin-coating method to achieve more ideal vertical phase separation for efficient charge transport and collection.[11–13] The sequential spin-coating method should offer more opportunities to individually optimize donor and acceptor layers through employing distinct solvents, solvent additives and post thermal or solvent

[a]Key Laboratory of Luminescence and Optical Information, Ministry of Education, Beijing Jiaotong University, Beijing, 100044, People's Republic of China. E-mail: fjzhang@bjtu.edu.cn; xlma2@bjtu.edu.cn

[b]Department of Applied Biology and Chemical Technology and Research Institute for Smart Energy, The Hong Kong Polytechnic University, Hung Hom, Hong Kong, China

[c]School of Physics, State Key Laboratory of Crystal Materials, Shandong University, Jinan, 250100, People's Republic of China

[d]Collaborative Innovation Center of Light Manipulations and Applications in Universities of Shandong, School of Physics and Electronics, Shandong Normal University, Jinan, 250014, People's Republic of China

[e]Organic Optoelectronic Materials Laboratory, Department of Chemistry, College of Science, Korea University, Seoul, 02841, Republic of Korea. E-mail: hywoo@korea.ac.kr

[f]Department of Physics, Beijing Technology and Business University, Beijing, 100048, People's Republic of China

[g]Tangshan Research Institute of Beijing Jiaotong University, Tangshan, 063000, People's Republic of China

† Electronic supplementary information (ESI) available. See DOI: https://doi.org/10.1039/d3ta07228b

‡ These authors contributed equally to this work.

treatment on each layer.[14–17] The additives, especially high boiling point solvent additives 1-chloronaphthalene (CN) and 1,8-diiodooctane (DIO), are commonly incorporated into the polymer acceptor solution. The polymer acceptors' aggregation degree, crystallinity and packing properties can be elaborately regulated during the slow volatilization of the solvent additive, leading to the performance improvement of QLA-PSCs.[18,19] It should be noticed that the high boiling point solvent additives are often difficult to completely volatilize during film processing, and the residual solvent additive may seriously affect the stability of QLA-PSCs. Alternatively, a series of solid additives are progressively developed in PSCs, which can maintain the advantages of controlling the active layer morphology, as well as presenting great potential in enhancing device stability with a simple post-treatment process.[20,21] The application of appropriate solid additives may be highly desirable for pushing the synergistic improvement of efficiency and stability for QLA-PSCs. Sun *et al.* reported the improved efficiency and stability of BHJ all-polymer solar cells by employing Y6 as a solid additive.[22] The typical works that employed additives to improve the performance of QLA-PSCs are summarized in Table 1. In this work, a nonfullerene acceptor as a solid additive is for the first time successfully applied in improving the performance of QLA-PSCs by deliberately selecting a nonfullerene acceptor having a similar chemical structure to the segment of polymer acceptor.

In this work, a series of QLA-PSCs were prepared with wide band gap polymer PM6 as a donor and narrow band gap polymer PY-IT as an acceptor, as well as L8-BO as a solid additive in the PY-IT layer. The chemical construction and energy level of the employed materials are presented in Fig. 1a. The L8-BO has a similar chemical structure to the segment of polymer acceptor PY-IT, which exhibits good potential for adjusting the molecular π–π stacking of PY-IT.[26–28] The normalized absorption spectra of neat and layered films are presented in Fig. 1b and c, respectively. The absorption spectra of layered films are normalized according to the absorption intensity of PM6. It is apparent that a slightly redshifted absorption peak and slightly enhanced absorption intensity of PY-IT can be simultaneously observed by incorporating L8-BO as a solid additive in layered films, which should be attributed to the close π–π stacking of PY-IT.[29,30] As shown in Fig. S1,† a similar phenomenon can also be observed from the absorption spectra of PY-IT films when processed with L8-BO as a solid additive, suggesting that the photon harvesting of the PY-IT layer can be improved by L8-BO. Meanwhile, interdiffusion between PM6 and PY-IT layers may be enhanced by incorporating L8-BO as a solid additive according to the contact angle experimental results, as displayed in Fig. 1d. The interfacial energy between the PM6 layer and PY-IT layer can be decreased from 3.32 mN $m^{-1}$ to 1.11 mN $m^{-1}$ by introducing L8-BO, and the surface and interfacial energies of the films are summarized in Table S1.† The decreased interfacial energy may facilitate molecular interdiffusion to achieve the expansion of the interface between the donor and acceptor, bringing about more efficient exciton dissociation in the PM6/PY-IT active layer.[31] The optimal PCE of 17.74% can be achieved with the introduction of 2 wt% L8-BO as a solid additive into the PY-IT layer, deriving from a simultaneously enhanced $J_{SC}$ of 24.45 mA $cm^{-2}$ and FF of 76.38%. Meanwhile, the optimized QLA-PSCs exhibit apparently improved stability with over 90.2% of their initial PCE being retained after storing in a glovebox for 2000 h. The effectiveness of the nonfullerene acceptor as a solid additive can also be verified from the improved PCEs of PM6/PY-IT based QLA-PSCs with Y6 or BO-4F as an additive. This work is the first case of improving the PCE and stability of QLA-PSCs by incorporating a nonfullerene acceptor as a solid additive.

## Results and discussion

The current density *versus* applied voltage (*J*–*V*) curves of the QLA-PSCs were measured under AM 1.5G illumination with 100 mW $cm^{-2}$ light intensity, as displayed in Fig. 2a. The key photovoltaic parameters of the QLA-PSCs are listed in Table 2. The PM6/PY-IT based QLA-PSCs exhibit a PCE of 16.14% with a $J_{SC}$ of 23.41 mA $cm^{-2}$, a $V_{OC}$ of 0.95 V and an FF of 72.60%. An optimal PCE of 17.74% can be achieved in QLA-PSCs with PM6/PY-IT:L8-BO (100 : 2, wt/wt) as active layers, deriving from a simultaneously enhanced $J_{SC}$ of 24.45 mA $cm^{-2}$ and FF of 76.38%, as well as the constant $V_{OC}$ of 0.95 V. A slightly

Table 1 The key photovoltaic parameters of QLA-PSCs without or with an additive[a]

| Additives | Active layers | $J_{SC}$ (mA $cm^{-2}$) | $V_{OC}$ (V) | FF (%) | PCE (%) | Ref. |
|---|---|---|---|---|---|---|
| Solvent additive | PBDB-T/PFBTz-TT | 17.74 | 0.86 | 51 | 7.78 | 19 |
| | PBDB-T/PFBTz-TT+CN | 18.95 | 0.85 | 63 | 10.14 | |
| | PBDB-T/PYT | 21.99 | 0.87 | 60.83 | 11.66 | 23 |
| | PBDB-T/PYT+CN | 23.03 | 0.89 | 73.98 | 15.17 | |
| | PBDB-T/PYT | 22.04 | 0.90 | 74 | 13.31 | 24 |
| | PBDB-T/PYT+CN | 23.07 | 0.91 | 77 | 16.05 | |
| | PM6/L15 | 22.48 | 0.95 | 60.23 | 12.35 | 18 |
| | PM6/L15+DIO | 22.99 | 0.95 | 68.69 | 14.28 | |
| | PM6/L15+CN | 23.58 | 0.94 | 73.17 | 16.15 | |
| | PM6/PY-V-γ+CN | 24.7 | 0.913 | 77.7 | 17.7 | 25 |
| Solid additive | PM6/PY-IT | 23.41 | 0.95 | 72.60 | 16.14 | This work |
| | PM6/PY-IT:L8-BO | 24.45 | 0.95 | 76.38 | 17.74 | |

[a] $J_{SC}$ is short circuit current density, $V_{OC}$ is open circuit voltage, and FF is fill factor.

 

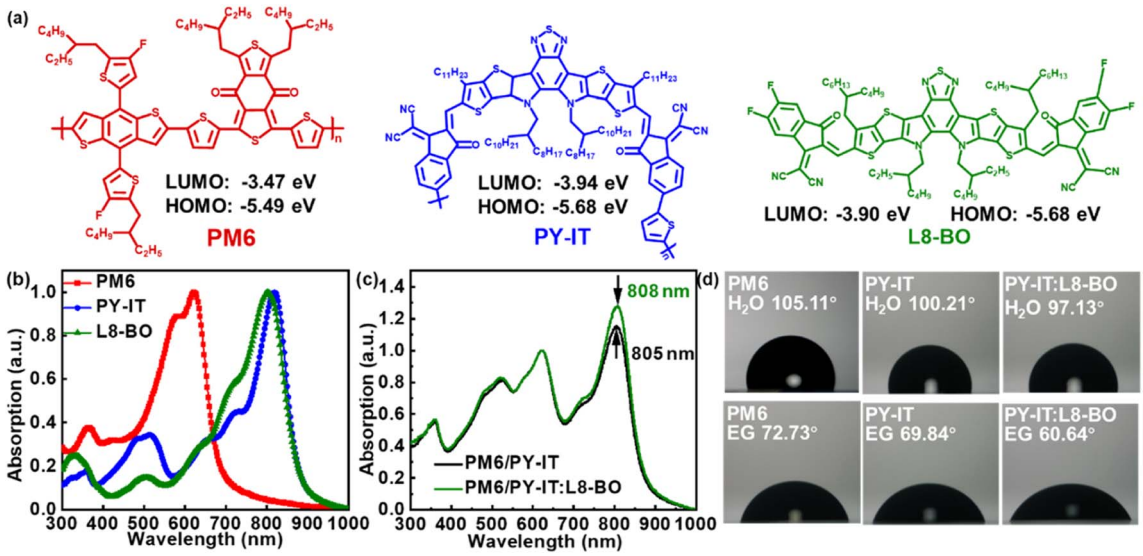


Fig. 1 (a) Chemical structures and energy level of PM6, PY-IT and L8-BO. (b) The normalized absorption spectra of PM6, PY-IT and L8-BO. (c) The absorption spectra of PM6/PY-IT and PM6/PY-IT:L8-BO films normalized according to the absorption intensity of PM6. (d) Images of contact angles of PM6, PY-IT and PY-IT:L8-BO films.

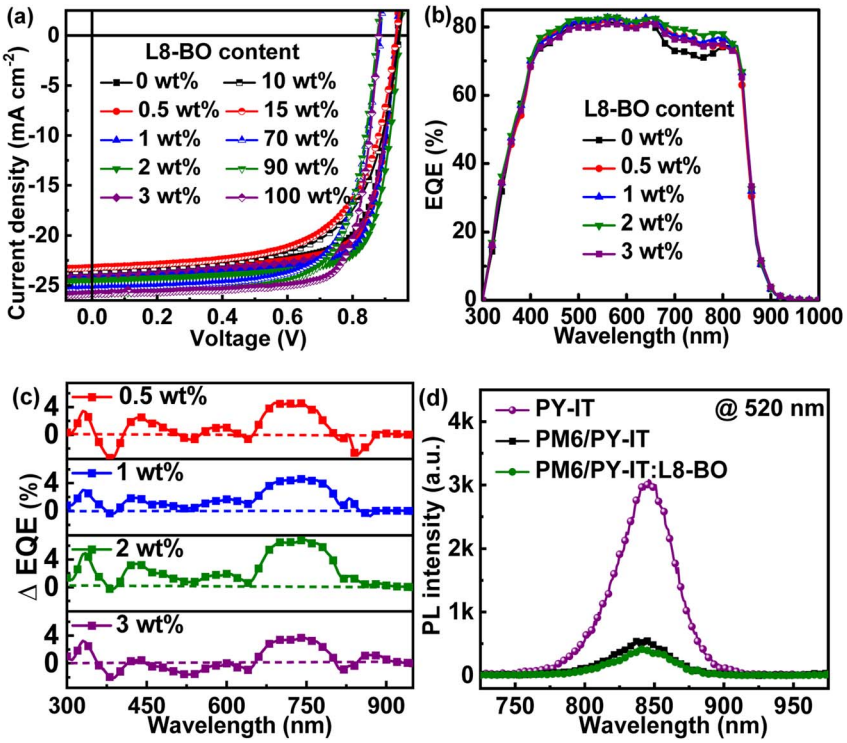


Fig. 2 (a) The $J$–$V$ curves of QLA-PSCs with different L8-BO content in the PY-IT layer. (b) The EQE spectra of QLA-PSCs with L8-BO as a solid additive in the PY-IT layer. (c) ΔEQE between corresponding QLA-PSCs. (d) PL spectra of neat PY-IT, PM6/PY-IT and PM6/PY-IT:L8-BO films.

increased PCE of 16.70% can also be kept until the incorporation content of L8-BO in PY-IT layers is less than 3 wt%. The QLA-PSCs exhibit markedly decreased FF and PCE values when the L8-BO content is larger than 10 wt% in PY-IT. According to the key parameters of QLA-PSC dependence on L8-BO content in PY-IT layers, less L8-BO in PY-IT should play the role of a solid additive rather than the third component. The external quantum efficiency (EQE) spectra of QLA-PSCs with L8-BO as a solid additive or a third component are presented in Fig. 2b and S2,† respectively. The calculated $J_{SC}$ can be obtained by integrating the corresponding EQE spectra, as listed in Table 2. The difference between measured $J_{SC}$ and calculated $J_{SC}$ values

Table 2 Key photovoltaic parameters of PM6/PY-IT based QLA-PSCs with different L8-BO content in the PY-IT layer[a]

| L8-BO function | L8-BO content [wt%] | *J*sc [mA cm$^{-2}$] | Calculated $J_{SC}$ [mA cm$^{-2}$] | *V*oc [V] | FF [%] | PCE (avg. ± dev.) [%] |
|---|---|---|---|---|---|---|
| Solid additive | 0 | 23.41 | 23.20 | 0.95 | 72.60 | 16.14 (15.91 ± 0.22) |
| | 0.5 | 23.84 | 23.39 | 0.95 | 73.77 | 16.71 (16.56 ± 0.17) |
| | 1 | 24.03 | 23.86 | 0.95 | 75.29 | 17.18 (16.98 ± 0.19) |
| | 2 | 24.45 | 24.09 | 0.95 | 76.38 | 17.74 (17.53 ± 0.21) |
| | 3 | 23.88 | 23.52 | 0.95 | 73.61 | 16.70 (16.47 ± 0.22) |
| Third component | 10 | 23.54 | 23.30 | 0.94 | 65.19 | 14.58 (14.45 ± 0.13) |
| | 15 | 23.22 | 23.02 | 0.93 | 64.19 | 13.86 (13.72 ± 0.14) |
| | 70 | 25.29 | 25.03 | 0.89 | 70.34 | 15.83 (15.72 ± 0.11) |
| | 90 | 25.79 | 25.54 | 0.88 | 71.10 | 16.14 (16.02 ± 0.12) |
| | 100 | 25.86 | 25.60 | 0.88 | 77.17 | 17.56 (17.34 ± 0.15) |

[a] The average and error values of PCE are from 10 individual cells.



should be mainly due to the decay of unencapsulated cells during EQE spectra measurement under air conditions. Obviously, the photon utilization efficiency of QLA-PSCs can be increased in the long wavelength region from 700 nm to 800 nm by incorporating L8-BO, which should be attributed to the enhanced photon harvesting by the lower L8-BO content. To intuitively evaluate the influence of L8-BO on photon utilization efficiency, the EQE spectral difference (ΔEQE) between PM6/PY-IT:L8-BO and PM6/PY-IT based QLA-PSCs is presented in Fig. 2c. It should be highlighted that ΔEQE values between those of the optimized and control QLA-PSCs are positive in the whole wavelength region, which may be related to the optimized PY-IT molecular arrangement and enlarged molecular interdiffusion for facilitating more efficient exciton separation. To confirm the positive effect of incorporating L8-BO on exciton dissociation in the PY-IT layer, the photoluminescence (PL) spectra of PY-IT, PM6/PY-IT and PM6/PY-IT:L8-BO films were measured, as shown in Fig. 2d. The pure PY-IT film presents a strong PL emission intensity with a characteristic peak at 845 nm. The PL emission of PY-IT is obviously quenched in the PM6/PY-IT film with a quenching efficiency of 81.47%, and the PL emission quenching of PY-IT is more pronounced in the PM6/PY-IT:L8-BO film with a quenching efficiency of 86.22%. The further quenched PL emission of the PY-IT:L8-BO film indicates that more PY-IT can permeate into the PM6 layer assisted by L8-BO as a solid additive, which can further support the enhanced EQE values in the whole wavelength region of the optimal QLA-PSCs.

To gain more insight into the impact of L8-BO as a solid additive on charge generation and extraction in active layers, the photogenerated current density ($J_{ph}$) *versus* effective voltage ($V_{eff}$) curves of the QLA-PSCs were recorded, as shown in Fig. 3a. The $J_{ph}$ can be described as $J_L$–$J_D$, where $J_L$ and $J_D$ represent the current density under standard illumination and in the dark. The $V_{eff}$ can be described as $V_0$–$V_a$, where $V_0$ is the voltage at $J_{ph}$ = 0 mA cm$^{-2}$ and $V_a$ is the applied voltage. The exciton dissociation efficiency ($\eta_D$) and charge collection efficiency ($\eta_C$) can be evaluated by $J^*_{ph}/J_{sat}$ and $J^{\&}_{ph}J_{sat}$, as shown in Table S2.† Here, $J^*_{ph}$, $J^{\&}_{ph}$ and $J_{sat}$ represent the $J_{ph}$ under short circuit and maximal power output conditions, as well as saturated photocurrent density, respectively.[32,33] The $\eta_D$ and $\eta_C$ values are 96.2% and 85.4% for the optimized QLA-PSCs, which are larger than the 95.4% and 84.2% for the PM6/PY-IT based QLA-PSCs. The synchronously enhanced $\eta_D$ and $\eta_C$ values result in the largest FF of 76.4% for the optimized QLA-PSCs. Transient photovoltage (TPV) measurement was performed on the QLA-PSCs to explore the charge recombination kinetics process, as shown in Fig. 3b.[34,35] The photocarrier lifetime ($\tau_{pho}$) can be extracted from TPV decay curves under open-circuit conditions. The $\tau_{pho}$ of the optimized QLA-PSCs is 18.11 μs, which is longer than the 8.74 μs for the PM6/PY-IT based QLA-PSCs. The prolonged $\tau_{pho}$ of the optimized QLA-PSCs indicates that charge recombination of active layers can be effectively suppressed by incorporating L8-BO as a solid additive. Charge extraction time ($\tau_{ext}$) can be evaluated from the transient photocurrent (TPC) decay curves under short-circuit conditions, as exhibited in Fig. 3c.[36–38] The $\tau_{ext}$ values are fitted to be 0.44 μs and 0.38 μs for the PM6/PY-IT and PM6/PY-IT:L8-BO based QLA-PSCs. The shorter $\tau_{ext}$ in the optimal QLA-PSCs indicates that the charge extraction process can be promoted to achieve the relatively large $\eta_C$ of 85.4%.

To further investigate the effects of L8-BO on charge transport and the recombination dynamic process of QLA-PSCs, electrochemical impedance spectroscopy (EIS) was employed in the frequency range from 30 Hz to 2 MHz at $V = V_{OC}$.[39,40] The Nyquist plots of the QLA-PSCs are displayed in Fig. 3d, and the inset shows the corresponding equivalent circuit model used to fit the Nyquist plot data. $R_{OS}$ represents the series resistance arising from the electrodes and bulk resistance in the active layer. $R_{CT}$ is defined as charge-transfer resistance, which is related to the interfacial charge transport process. The constant phase element (CPE) is introduced into the circuit model to compensate for interface inhomogeneity in active layers. The CPE can be defined by $CPE_T$ and $CPE_P$, where the $CPE_T$ represents the capacitance value and $CPE_P$ is the inhomogeneous constant changing from 0 and 1. When $CPE_P$ is equal to 1, the CPE plays the role of an ideal capacitor without any defects.[41] The corresponding parameters of QLA-PSCs are summarized in Table S3.† The $R_{OS}$ and $R_{CT}$ values for the optimized QLA-PSCs are 31.7 Ω and 35.2 Ω, which are smaller than those of 32.6 Ω and 37.1 Ω for the PM6/PY-IT based QLA-PSCs. The reduced $R_{OS}$ and $R_{CT}$ values of the optimized QLA-PSCs indicate that the incorporated L8-BO should promote charge transport and

 

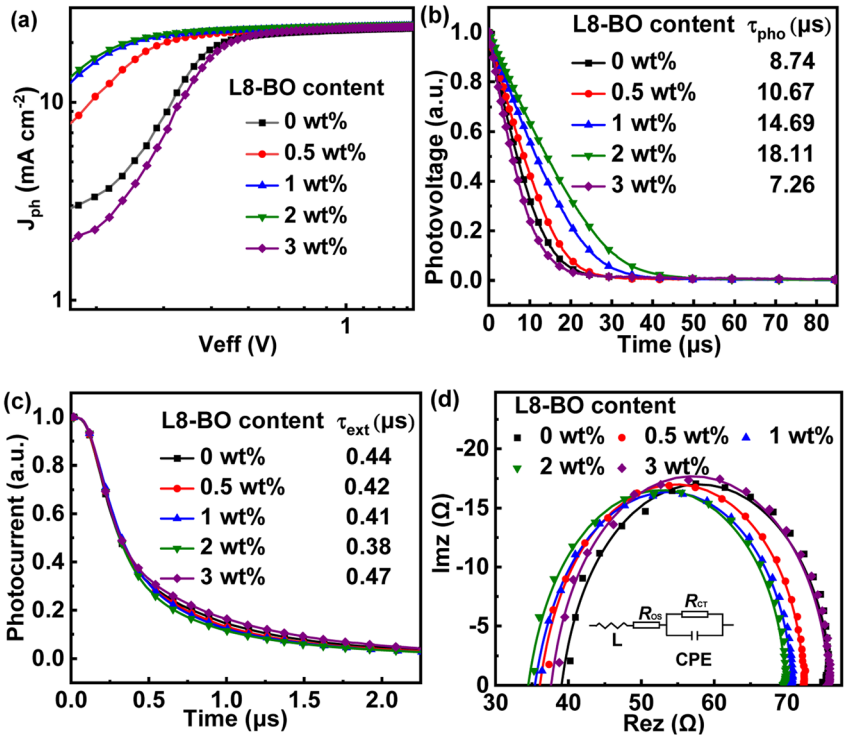


Fig. 3 (a) $J_{ph}$–$V_{eff}$ curves, (b) transient photovoltage curves, (c) transient photocurrent curves and (d) Nyquist plots and equivalent circuit of QLA-PSCs.

suppress charge recombination in active layers. The $CPE_P$ values are 0.958 and 0.990 for the PM6/PY-IT based and the optimized QLA-PSCs. The $CPE_P$ value of the optimized QLA-PSCs being closer to 1 suggests that the interfacial capacitance should be more electrically ideal in QLA-PSCs with L8-BO incorporation. The average carrier lifetime ($\tau$) in active layers can be calculated based on the equation: $\tau = R_{CT} \times CPE_T$. The $\tau$ values are estimated to be 438 and 269 ns for QLA-PSCs without and with L8-BO, respectively. The shorter $\tau$ value of the optimized QLA-PSCs indicates that charge recombination in the active layers can be effectively inhibited by incorporating L8-BO as a solid additive. The space charge limited current (SCLC) method was employed to assess the incorporation of L8-BO as a solid additive on electron mobility ($\mu_e$) in the PY-IT layer.[42,43] The $\ln(JL^3/V^2) - (V/L)^{0.5}$ curves of the electron-only devices are depicted in Fig. S3.† The $\mu_e$ values of PY-IT and PY-IT:L8-BO films are $4.53 \times 10^{-4}$ and $6.18 \times 10^{-4}$ cm$^2$ V$^{-1}$ s$^{-1}$, respectively. The enhanced $\mu_e$ in the PY-IT layer can rationalize the increased FF of the optimal QLA-PSCs.

Transient absorption (TA) spectroscopy was employed to characterize the hole transfer and exciton diffusion dynamic process in layered films. As shown in Fig. S4,† the ground state bleaching (GSB) peaks of neat PM6 films are centered at ~620 nm, which correspond well with the steady absorption spectra of the corresponding neat films.[44] The PY-IT presents a relatively broad GSB signal with characteristic peaks at ~710 nm and ~800 nm. The TA spectra of the PM6/PY-IT and PM6/PY-IT:L8-BO films at different probe delay times are displayed in Fig. 4a and b. The PY-IT can be selectively excited in the PM6/PY-IT and PM6/PY-IT:L8-BO layered films by setting the long pump wavelength to 800 nm. The GSB characteristic peak probed at ~620 nm emerged in layered films when pumped with 800 nm light, implying the existence of a hole transfer process from PY-IT to PM6.[45] The exciton diffusion length ($L_D$) for PY-IT can be estimated according to the fluence dependent TA spectra of the corresponding films, as displayed in Fig. 4c and d. The dynamic decay of the excitons can be described based on the following equation: $\frac{dn(t)}{dt} = -kn(t) - \frac{1}{2}\gamma n^2(t)$, which involves monomolecular recombination and exciton–exciton annihilation. The solution of the equation is $n(t) = \frac{n(0)e^{(-kt)}}{1 + \frac{\gamma}{k}n(0)[1 - e^{(-kt)}]}$, in which $n(t)$ is the density of excitons as the function of decay time $t$, $k$ represents the monomolecular decay rate constant, and $\gamma$ is the singlet–singlet bimolecular exciton annihilation rate. The $k$ values are fixed at $0.750 \times 10^9$ and $0.735 \times 10^9$ s$^{-1}$ for the PY-IT film and PY-IT:L8-BO film, respectively. The $L_D$ can be calculated according to the equation $L_D = \sqrt{D\tau}$. In this equation, $\tau$ is the lifetime of the exciton equal to $1/k$, and $D$ represents the exciton diffusion coefficients obtained through $D = \frac{\gamma}{4\pi R}$, where $R$ is the annihilation radius of singlet excitons (~2 nm).[46] The detailed fitting parameters of the PY-IT film and PY-IT:L8-BO film are summarized in Table S4.† The calculated $L_D$ values of the PY-IT and PY-IT:L8-BO films are 8.79 and 9.07 nm, respectively. The extended $L_D$ values of the PY-IT:L8-BO film should allow more excitons generated in the acceptor phase to move to the donor :

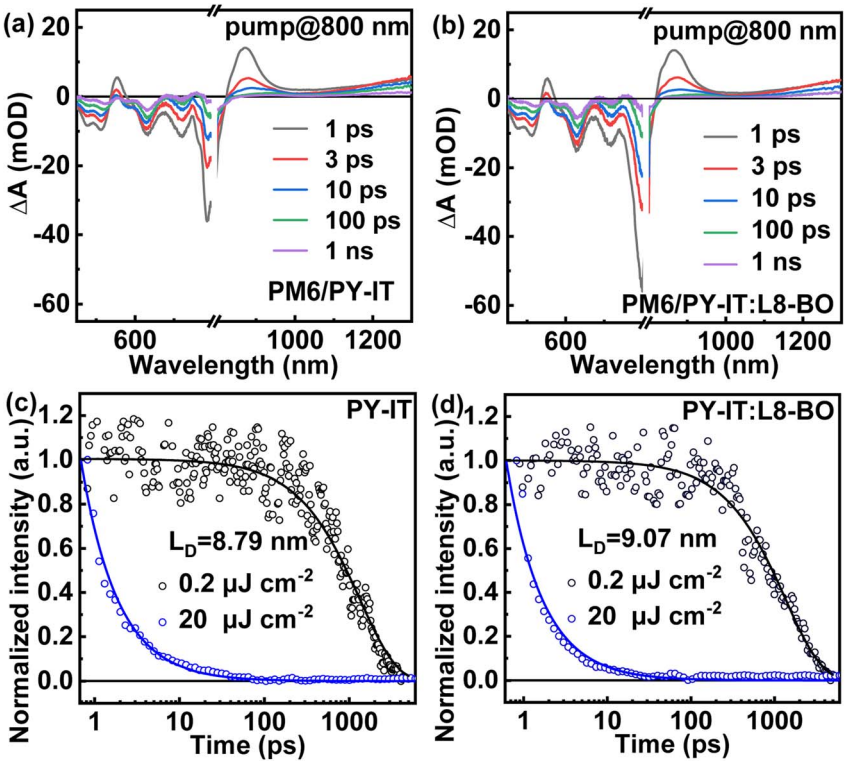


Fig. 4 TA spectra of (a) the PM6/PY-IT film and (b) PM6/PY-IT:L8-BO film at different probe delay times. Pump-fluence dependent TA kinetics of (c) the PY-IT film and (d) PY-IT: L8-BO film traced at 875 nm.

acceptor interface for dissociation, contributing to $J_{SC}$ improvement of the optimal QLA-PSCs.

Grazing-incidence wide-angle X-ray scattering (GIWAXS) characterization was performed to further explore the effect of L8-BO incorporation on the molecular arrangement of films. Fig. S5† shows the 2D GIWAXS patterns and 1D line-cut profiles of the neat PM6 and PY-IT films. The (100) and (010) diffraction peaks in both out-of-plane (OOP) and in-plane (IP) directions can be concurrently observed from the neat PM6 film, indicating the coexistence of face-on and edge-on molecular orientation of PM6. The neat PY-IT film exhibits obvious OOP (010) and IP (100) diffraction peaks, indicating the preferred face-on orientation in the neat PY-IT film. The 2D GIWAXS patterns and corresponding 1D line-cut profiles of the layered films are displayed in Fig. 5a and b, respectively. The OOP (010) diffraction peaks of the layered films are located at 1.62 $Å^{-1}$, which is between those at 1.60 $Å^{-1}$ for the PY-IT film and 1.64 $Å^{-1}$ for the PM6 film, revealing that the π–π stacking in layered films is associated with PM6 and PY-IT. The IP (100) and OOP (010) diffraction peak intensity of the layered films can be significantly increased by incorporating L8-BO, manifesting the formation of a more ordered face-on orientation of PY-IT.[47,48] The well-regulated face-on packing of PY-IT should be beneficial to electron transport along the direction perpendicular to the substrate, contributing to FF improvement of the optimal QLA-PSCs.

The long-term stability of the control and optimized QLA-PSCs was monitored with the cells stored in a high purity $N_2$ filled glovebox. As shown in Fig. 6a, the optimal PM6/PY-IT:L8-BO based QLA-PSCs can retain 90.2% of their initial PCE after 2000 h of storage, which is apparently larger than the 85.1% for the PM6/PY-IT based QLA-PSCs under the same conditions. The thermal and light soaking stabilities of the QLA-PSCs in a high purity $N_2$ filled glovebox are shown in Fig. S6.† The PM6/PY-IT and PM6/PY-IT:L8-BO based QLA-PSCs can maintain 89.94% and 91.62% of the initial PCE after 350 h of heating at 65 °C, respectively. Moreover, the preserved percentage of the initial PCE is 90.27% or 91.10% for the QLA-PSCs based on PM6/PY-IT or PM6/PY-IT:L8-BO as the active layers under AM 1.5G illumination of 100 mW $cm^{-2}$ for 270 min. The obviously improved stability of the QLA-PSCs by incorporating 2 wt% L8-BO as a solid additive should be mainly ascribed to the more ordered molecular stacking in the PY-IT films.[49] To further verify the effect of the universality of non-fullerene materials as solid additives on the performance improvement of QLA-PSCs, the other two non-fullerene materials Y6 and BO-4F were also incorporated into the PY-IT layer.[50,51] The *J*–*V* curves and PCE of the corresponding QLA-PSCs are presented in Fig. 6b. The key photovoltaic parameters of the QLA-PSCs are listed in Table S5.† The PCE of the QLA-PSCs can be increased from 16.14% to 16.71% or 16.79% by incorporating Y6 or BO-4F as a solid additive, accompanied by the simultaneously increased $J_{SC}$ and FF. The universality of non-fullerene

 

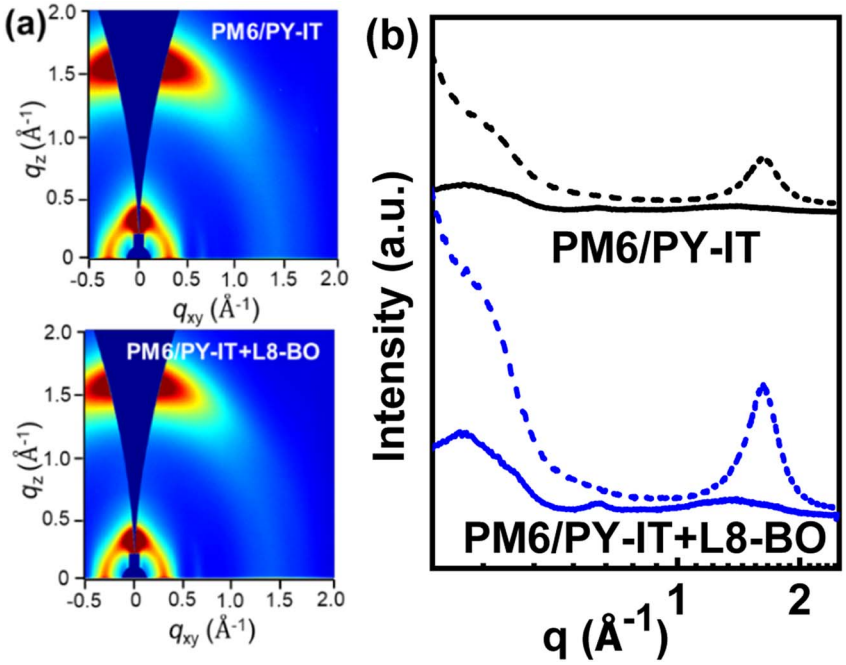


Fig. 5 (a) The 2D-GIWAXS patterns of the PM6/PY-IT and PM6/PY-IT:L8-BO films; (b) the out-of-plane (dotted lines) and in-plane (solid lines) line-cut profiles abstracted from the 2D GIWAXS images.

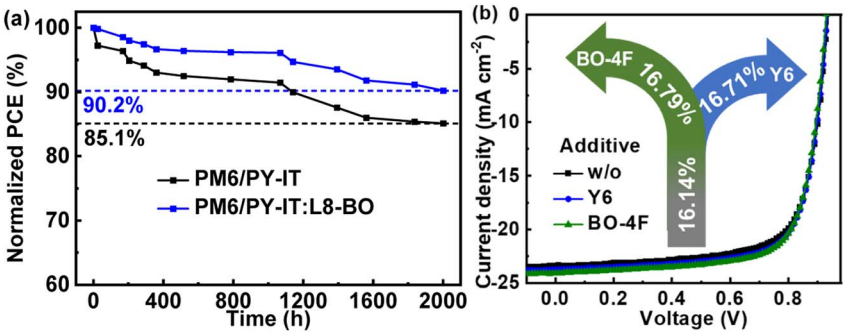


Fig. 6 (a) The normalized PCEs of QLA-PSC dependence on time of the storage stability in an $N_2$ filled glovebox. (b) The $J$–$V$ curves of QLA-PSCs with different solid additives.

materials as solid additives can be further confirmed, which may provide a novel strategy to improve the performance of QLA-PSCs.

## Conclusion

In summary, based on polymer donor PM6 and polymer acceptor PY-IT, a series of QLA-PSCs processed without or with solid additive L8-BO were constructed by the spin-coating method. The optimal PCE of 17.74% was achieved in QLA-PSCs with 2 wt% L8-BO incorporated into the PY-IT layer, benefiting from the enhanced $J_{SC}$ of 24.45 mA cm$^{-2}$ and FF of 76.38%. To our knowledge, the PCE of 17.74% should be among the top values for QLA-PSCs. The increased $J_{SC}$ of the optimal QLA-PSCs is primarily due to the enlarged exciton diffusion length as well as the increased exciton dissociation interface induced by solid additive L8-BO. The L8-BO can also act as a morphology regulator to improve molecular aggregation and packing for realizing effective electron transport in active layers, delivering an FF increment for the optimal QLA-PSCs. It is noteworthy that excellent long-term stability can be realized in the optimal QLA-PSCs, which can retain 90.2% of the primeval PCE after 2000 h of storage in an $N_2$ filled glovebox. This work demonstrates that using a small molecular nonfullerene acceptor as a solid additive should be a facile and effective strategy to achieve QLA-PSCs with high efficiency and superior long-term stability.

## Author contributions

W. Xu and M. Zhang carried out the device fabrication and characterization. X. Ma, H. Woo and F. Zhang designed the experiments. Z. Liu and H. Tian also took part in the experiments. W. Zhang and X. Hao performed the TA characterizations. S. Sun and Q. Sun analyzed the PL data. S. Jeong

carried out the GIWAXS analysis. F. Zhang and X. Li carried out the TPV and TPC experiments. All authors discussed the results and commented on the manuscript.

## Conflicts of interest

There are no conflicts of interest to declare.

## Acknowledgements

This work was supported by the Fundamental Research Funds for the Central Universities (2022YJS104); Natural Science Foundation of Beijing (4232073 and 1232029); National Natural Science Foundation of China (Grant No. 62175011, 62205276, 62105017 and 52311540151); Natural Science Foundation of Hebei Province (F2023105002); and Chunhui Project Foundation of the Education Department of China (HZKY20220002).

## References

1 R. Zeng, L. Zhu, M. Zhang, W. Zhong, G. Zhou, J. Zhuang, T. Hao, Z. Zhou, L. Zhou, N. Hartmann, X. Xue, H. Jing, F. Han, Y. Bai, H. Wu, Z. Tang, Y. Zou, H. Zhu, C. Chen, Y. Zhang and F. Liu, *Nat. Commun.*, 2023, **14**, 4148.
2 T. Chen, X. Zheng, D. Wang, Y. Zhu, Y. Ouyang, J. Xue, M. Wang, S. Wang, W. Ma, C. Zhang, Z. Ma, S. Li, L. Zuo and H. Chen, *Adv. Mater.*, 2023, **35**, 2308061.
3 R. Sun, T. Wang, Q. Fan, M. Wu, X. Yang, X. Wu, Y. Yu, X. Xia, F. Cui, J. Wan, X. Lu, X. Hao, A. K. Y. Jen, E. Spiecker and J. Min, *Joule*, 2023, **7**, 221–237.
4 X. Li, X. Duan, J. Qiao, S. Li, Y. Cai, J. Zhang, Y. Zhang, X. Hao and Y. Sun, *Adv. Energy Mater.*, 2022, **13**, 2203044.
5 T. Zhang, Y. Xu, H. Yao, J. Zhang, P. Bi, Z. Chen, J. Wang, Y. Cui, L. Ma, K. Xian, Z. Li, X. Hao, Z. Wei and J. Hou, *Energy Environ. Sci.*, 2023, **16**, 1581–1589.
6 R. Ma, Q. Fan, T. Dela, B. Wu, H. Liu, Q. Wu, Q. Wei, J. Wu, X. Lu, M. Li, W. Ma and G. Li, *Adv. Mater.*, 2023, **35**, 2212275.
7 L. Zhu, M. Zhang, J. Xu, C. Li, J. Yan, G. Zhou, W. Zhong, T. Hao, J. Song, X. Xue, Z. Zhou, R. Zeng, H. Zhu, C. Chen, R. MacKenzie, Y. Zou, J. Nelson, Y. Zhang, Y. Sun and F. Liu, *Nat. Mater.*, 2022, **21**, 656–663.
8 L. Zhan, S. Li, Y. Li, R. Sun, J. Min, Y. Chen, J. Fang, C. Ma, G. Zhou, H. Zhu, L. Zuo, H. Qiu, S. Yin and H. Chen, *Adv. Energy Mater.*, 2022, **12**, 2201076.
9 D. Chen, S. Liu, B. Huang, J. Oh, F. Wu, J. Liu, C. Yang, L. Chen and Y. Chen, *Small*, 2022, **18**, 2200734.
10 Z. Yao, X. Wan, C. Li and Y. Chen, *Acc. Mater. Res.*, 2023, **4**, 772–785.
11 Y. Wei, Z. Chen, G. Lu, N. Yu, C. Li, J. Gao, X. Gu, X. Hao, G. Lu, Z. Tang, J. Zhang, Z. Wei, X. Zhang and H. Huang, *Adv. Mater.*, 2022, **34**, 2204718.
12 J. Han, H. Xu, S. Paleti, Y. Wen, J. Wang, Y. Wu, F. Bao, C. Yang, X. Li, X. Jian, J. Wang, S. Karuthedath, J. Gorenflot, F. Laquai, D. Baran and X. Bao, *ACS Energy Lett.*, 2022, **7**, 2927–2936.
13 L. Wen, H. Mao, L. Zhang, J. Zhang, Z. Qin, L. Tan and Y. Chen, *Adv. Mater.*, 2023, **25**, 2308159.
14 W. Xu, X. Zhu, X. Ma, H. Zhou, X. Li, S. Jeong, H. Woo, Z. Zhou, Q. Sun and F. Zhang, *J. Mater. Chem. A*, 2022, **10**, 13492–13499.
15 G. Cai, Z. Chen, X. Xia, Y. Li, J. Wang, H. Liu, P. Sun, C. Li, R. Ma, Y. Zhou, W. Chi, J. Zhang, H. Zhu, J. Xu, H. Yan, X. Zhan and X. Lu, *Adv. Sci.*, 2022, **9**, 2200578.
16 Y. Zheng, R. Sun, M. Zhang, Z. Chen, Z. Peng, Q. Wu, X. Yuan, Y. Yu, T. Wang, Y. Wu, X. Hao, G. Lu, H. Ade and J. Min, *Adv. Energy Mater.*, 2021, **11**, 2102135.
17 S. Bao, H. Yang, H. Fan, J. Zhang, Z. Wei, C. Cui and Y. Li, *Adv. Mater.*, 2021, **33**, 2105301.
18 B. Li, X. Zhang, Z. Wu, J. Yang, B. Liu, Q. Liao, J. Wang, K. Feng, R. Chen, H. Y. Woo, F. Ye, L. Niu, X. Guo and H. Sun, *Sci. China Chem.*, 2022, **65**, 1157–1163.
19 B. Wu, Y. Zhang, S. Tian, J. Oh, M. Yang, L. Pan, B. Yin, C. Yang, C. Duan, F. Huang and Y. Cao, *Sol. RRL*, 2022, **6**, 2101034.
20 J. Song, Y. Li, Y. Cai, R. Zhang, S. Wang, J. Xin, L. Han, D. Wei, W. Ma, F. Gao and Y. Sun, *Matter*, 2022, **5**, 4047–4059.
21 L. Zhong, Z. Sun, S. Lee, S. Jeong, S. Jung, Y. Cho, J. Park, J. Park, S. Yoon and C. Yang, *Adv. Funct. Mater.*, 2023, **33**, 2305450.
22 Z. Ge, J. Qiao, Y. Li, J. Song, C. Zhang, Z. Fu, M. Jee, X. Hao, H. Woo and Y. Sun, *Adv. Mater.*, 2023, **35**, 2301906.
23 Q. Wu, W. Wang, Y. Wu, Z. Chen, J. Guo, R. Sun, J. Guo, Y. Yang and J. Min, *Adv. Funct. Mater.*, 2021, **31**, 2010411.
24 Y. Zhang, B. Wu, Y. He, W. Deng, J. Li, J. Li, N. Qiao, Y. Xing, X. Yuan, N. Li, C. Brabec, H. Wu, G. Lu, C. Duan, F. Huang and Y. Cao, *Nano Energy*, 2022, **93**, 106858.
25 Y. Wang, H. Yu, X. Wu, D. Zhao, S. Zhang, X. Zou, B. Li, D. Gao, Z. Li, X. Xia, X. Chen, X. Lu, H. Yan, C. Chueh, A. Jen and Z. Zhu, *Adv. Energy Mater.*, 2022, **12**, 2202729.
26 Z. Luo, T. Liu, R. Ma, Y. Xiao, L. Zhan, G. Zhang, H. Sun, F. Ni, G. Chai, J. Wang, C. Zhong, Y. Zou, X. Guo, X. Lu, H. Chen, H. Yan and C. Yang, *Adv. Mater.*, 2020, **32**, 2005942.
27 C. Li, J. Zhou, J. Song, J. Xu, H. Zhang, X. Zhang, J. Guo, L. Zhu, D. Wei, G. Han, J. Min, Y. Zhang, Z. Xie, Y. Yi, H. Yan, F. Gao, F. Liu and Y. Sun, *Nat. Energy*, 2021, **6**, 605–613.
28 H. Zhang, M. Liu, X. Zhao, X. Ma, G. Yuan, J. Li and F. Zhang, *Appl. Phys. Lett.*, 2023, **123**, 111101.
29 L. Ma, Y. Cui, J. Zhang, K. Xian, Z. Chen, K. Zhou, T. Zhang, W. Wang, H. Yao, S. Zhang, X. Hao, L. Ye and J. Hou, *Adv. Mater.*, 2022, **34**, 2208926.
30 J. Zhao, S. Chung, H. Li, Z. Zhao, C. Zhu, J. Yin, K. Cho and Z. Kan, *Adv. Funct. Mater.*, 2023, **33**, 2307355.
31 X. Ma, A. Zeng, J. Gao, Z. Hu, C. Xu, J. H. Son, S. Y. Jeong, C. Zhang, M. Li, K. Wang, H. Yan, Z. Ma, Y. Wang, H. Woo and F. Zhang, *Natl. Sci. Rev.*, 2021, **8**, nwaa305.
32 C. Yang, M. Jiang, S. Wang, B. Zhang, P. Mao, H. Woo, F. Zhang, J. Wang and Q. An, *Adv. Mater.*, 2023, **35**, 2305356.
33 Z. Liu, M. Zhang, L. Zhang, S. Jeong, S. Geng, H. Woo, J. Zhang, F. Zhang and X. Ma., *Chem. Eng. J.*, 2023, **471**, 144711.
34 W. Gao, T. Liu, R. Sun, G. Zhang, Y. Xiao, R. Ma, C. Zhong, X. Lu, J. Min, H. Yan and C. Yang, *Adv. Sci.*, 2020, **7**, 1902657.

 

35 P. Bi, J. Wang, Y. Cui, J. Zhang, T. Zhang, Z. Chen, J. Qiao, J. Dai, S. Zhang, X. Hao, Z. Wei and J. Hou, *Adv. Mater.*, 2023, **35**, 2210865.
36 W. Xu, X. Li, S. Jeong, J. Son, Z. Zhou, Q. Jiang, H. Woo, Q. Wu, X. Zhu, X. Ma and F. Zhang, *J. Mater. Chem. C*, 2022, **10**, 5489–5496.
37 W. Dong, Z. Qin, K. Wang, Y. Xiao, X. Liu, S. Ren and L. Li, *Angew. Chem., Int. Ed.*, 2023, **62**, e202216073.
38 X. Zhao, Q. An, H. Zhang, C. Yang, A. Mahmood, M. Jiang, M. Jee, B. Fu, S. Tian, H. Woo, Y. Wang and J. Wang, *Angew. Chem., Int. Ed.*, 2023, **62**, e202216340.
39 W. Xu, M. Zhang, X. Ma, X. Zhu, S. Jeong, H. Woo, J. Zhang, W. Du, J. Wang, X. Liu and F. Zhang, *Adv. Funct. Mater.*, 2023, **33**, 2215204.
40 H. Bai, Q. An, M. Jiang, H. Ryu, J. Yang, X. Zhou, H. Zhi, C. Yang, X. Li, H. Woo and J. Wang, *Adv. Funct. Mater.*, 2022, **32**, 2200807.
41 X. Ma, Q. Jiang, W. Xu, C. Xu, S. Jeong, H. Woo, Q. Wu, X. Zhang, G. Yuan and F. Zhang, *Chem. Eng. J.*, 2022, **442**, 136368.
42 M. Jiang, H. Zhi, B. Zhang, C. Yang, A. Mahmood, M. Zhang, H. Woo, F. Zhang, J. Wang and Q. An, *ACS Energy Lett.*, 2023, **8**, 1058–1067.
43 W. Xu, X. Ma, J. Son, S. Jeong, L. Niu, C. Xu, S. Zhang, Z. Zhou, J. Gao, H. Woo, J. Zhang, J. Wang and F. Zhang, *Small*, 2022, **18**, 2104215.
44 J. Grüne, G. Londi, A. Gillett, B. Stähly, S. Lulei, M. Kotova, Y. Olivier, V. Dyakonov and A. Sperlich, *Adv. Funct. Mater.*, 2023, **33**, 2212640.
45 F. Cui, Z. Chen, J. Qiao, T. Wang, G. Lu, H. Yin and X. T. Hao, *Adv. Funct. Mater.*, 2022, **32**, 2200478.
46 P. Bi, S. Zhang, J. Ren, Z. Chen, Z. Zheng, Y. Cui, J. Wang, S. Wang, T. Zhang, J. Li, Y. Xu, J. Qin, C. An, W. Ma, X. Hao and J. Hou, *Adv. Mater.*, 2022, **34**, 2108090.
47 M. Liu, X. Ge, X. Jiang, F. Guo, S. Gao, Q. Peng, L. Zhao and Y. Zhang, *Adv. Funct. Mater.*, 2023, **33**, 2300214.
48 X. Ma, W. Xu, Z. Liu, S. Y. Jeong, C. Xu, J. Zhang, H. Woo, Z. Zhou and F. Zhang, *ACS Appl. Mater. Interfaces*, 2023, **15**, 7247–7254.
49 R. Sun, Y. Wu, X. Yang, Y. Gao, Z. Chen, K. Li, J. Qiao, T. Wang, J. Guo, C. Liu, X. Hao, H. Zhu and J. Min, *Adv. Mater.*, 2022, **34**, 2110147.
50 J. Yuan, Y. Zhang, L. Zhou, G. Zhang, H. Yip, T. Lau, X. Lu, C. Zhu, H. Peng, P. Johnson, M. Leclerc, Y. Cao, J. Ulanski, Y. Li and Y. Zou, *Joule*, 2019, **3**, 1140–1151.
51 A. Wang, Y. Kang, C. Hou, R. Li, Y. Song and Q. Dong, *Sci. Bull.*, 2023, **68**, 1153–1161.